Lawrence Berkeley National Laboratory

LBL Publications

Title

On the chemical homogeneity of InxGa1−xN alloys – Electron microscopy at the edge of technical limits

Permalink

https://escholarship.org/uc/item/1r52597n

Authors

Specht, Petra
Kisielowski, Christian

Publication Date

2017-07-01

DOI

10.1016/j.mssp.2016.07.011

Peer reviewed

eScholarship.org Powered by the California Digital Library
University of California

Materials Science in Semiconductor Processing 65 (2017) 24–34

Contents lists available at ScienceDirect

Materials Science in Semiconductor Processing

journal homepage: www.elsevier.com/locate/mssp

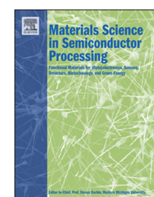

Review

On the chemical homogeneity of $In_xGa_{1-x}N$ alloys – Electron microscopy at the edge of technical limits

Petra Specht [a,*], Christian Kisielowski [b]

[a] Department of Materials Science & Engineering, University of California-Berkeley, Berkeley, CA 94720, USA
[b] Molecular Foundry, Lawrence Berkeley National Laboratories, Berkeley, CA 94720, USA

ARTICLE INFO

Article history:
Received 30 March 2016
Received in revised form
25 May 2016
Accepted 20 July 2016
Available online 31 August 2016

Keywords:
Transmission electron microscopy
$In_xGa_{1-x}N$ alloys
Homogeneity
Spinodal decomposition
Band gap

ABSTRACT

Ternary $In_xGa_{1-x}N$ alloys became technologically attractive when p-doping was achieved to produce blue and green light emitting diodes (LED)s. Starting in the mid 1990th, investigations of their chemical homogeneity were driven by the need to understand carrier recombination mechanisms in optical device structures to optimize their performance. Transmission electron microscopy (TEM) is the technique of choice to complement optical data evaluations, which suggests the coexistence of local carrier recombination mechanisms based on piezoelectric field effects and on indium clustering in the quantum wells of LEDs. We summarize the historic context of homogeneity investigations using electron microscopy techniques that can principally resolve the question of indium segregation and clustering in $In_xGa_{1-x}N$ alloys if optimal sample preparation and electron dose-controlled imaging techniques are employed together with advanced data evaluation.
© 2016 The Authors. Published by Elsevier Ltd. This is an open access article under the CC BY license (http://creativecommons.org/licenses/by/4.0/).

Contents

1. Background . . . 24
2. Quantification of indium clusters . . . 26
 2.1. Pattern recognition . . . 26
 2.2. Strain mapping . . . 27
 2.3. Contrast quantification of single atom columns . . . 29
3. Improving the existing electron microscopy capabilities . . . 31
 3.1. FIB sample preparation . . . 31
 3.2. Valence electron energy loss spectroscopy (VEELS) . . . 31
 3.3. Prospects for aberration-corrected microscopy . . . 31
 3.4. What is the atomic structure of “indium clusters”? . . . 32
4. Conclusions . . . 33
Acknowledgments . . . 33
References . . . 33

1. Background

The ternary $In_xGa_{1-x}N$ material system became well-known in the early 1990th with the development of blue and green LEDs in Japan. While I. Akasaki and H. Amano were working at Nagoya University, S. Nakamura pushed the development of GaN-based LEDs at Tokushima based Nichia Inc. All three researchers received the Nobel Prize in Physics 2014, for their respective “achievements in the development of the highly energy efficient blue LED which led to the emergence of white light” [1]. Amano and Akasaki discovered hydrogen passivation which de-activated p-doping in Mg-doped GaN after treating it with low-energy electron beam irradiation, therewith locally heating it [2]. Activating p-doping with an annealing step enabled the production of GaN-based photo diodes. This discovery was not the only reason, though, that the history of $In_xGa_{1-x}N$ alloy development was from the very

* Corresponding author.
E-mail address: specht@berkeley.edu (P. Specht).

http://dx.doi.org/10.1016/j.mssp.2016.07.011
1369-8001/© 2016 The Authors. Published by Elsevier Ltd. This is an open access article under the CC BY license (http://creativecommons.org/licenses/by/4.0/).

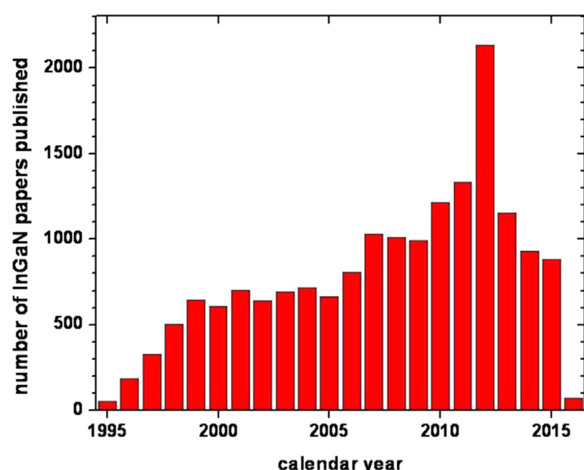

Fig. 1. Number of $In_xGa_{1-x}N$ based research papers per year, from the Web of Knowledge [14].

beginning closely connected to electron microscopy investigations.

The growth of pure GaN is already challenging due to lack of a suitable, lattice matched substrate [3]. Most electronic structures are grown on sapphire or SiC; growth on silicon is very desirable for device integration. For opto-electronic applications the transparent and inexpensive sapphire is often used. Various growth techniques were tried with MOCVD, MOVPE and MBE being the most prominent among them. The lattice mismatch due to the different materials' lattice constants, but also due to variations in the thermal expansion coefficients during the cooling of the hetero-structures commonly results in high dislocation densities (for MOCVD growth 10^8–$10^9/cm^2$ is typical) and residual strain in the epilayers [4,5]. The group III – nitride system also exhibits piezoelectric effects which can lead to internal charge separation, an effect which is exploited in AlGaN/GaN high electron mobility transistors (HEMTs). In order to achieve highly efficient $In_xGa_{1-x}N$ LED structures carrier recombination mechanisms need to be identified. In this context it was diversely discussed if the piezoelectric effect, resulting in a quantum confined Stark effect (QCSE) or the local presence of indium enriched $In_xGa_{1-x}N$ clusters in the quantum wells of a LED were dominating optical devices' properties. While the first effect promotes a carrier separation in a locally changed band structure, the second effect locally confines carrier recombination in In-rich clusters. Both effects will produce a "red shift" in energy, resulting in an energy reduction of the optical response, but their temporal and excitation dependence differs [6]. A combination of structural and optical characterization suggested the coexistence of both mechanisms [6]. The existence of a phase separation in the $In_xGa_{1-x}N$ alloy system was suggested as early as 1996 [7]. However, there was only partial agreement on physical models for an interpretation of emission spectra [8–10]. Moreover, efforts were made to kinematically suppress phase separation under specific growth conditions (see for example refs [11,12] for recent efforts in this direction). Thus, clarifying the question how indium is distributed in the GaN lattice is an essential task in the effort to understand optical device performance that is needed to improve the internal device efficiency described in 1995 [13]. The growth of $In_xGa_{1-x}N$ quantum well (QW) structures as required for blue LEDs was already . In the following years the number of $In_xGa_{1-x}N$ related publications literally exploded as researchers from all over the world started working in this field. Fig. 1 displays the total number of papers published per year addressing $In_xGa_{1-x}N$ research as documented in the "Web of Knowledge" [14]. A sharp increase of publications is observed in 2012 that may relate to reports that internal efficiencies can be improved for green LED's by suitably shaping the indium distribution in graded quantum wells (see for example [15]). However, the issue remains unresolved to date.

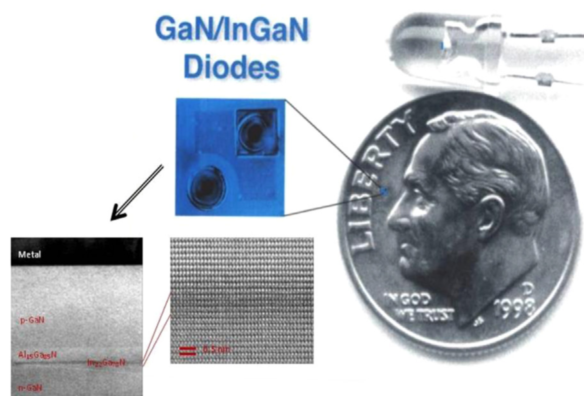

Fig. 2. Schematic of reverse engineering of a blue (green) LED, to produce TEM cross-sectional samples, the AlGaN layer in the TEM sample is about 30 nm thick, other dimensions are described in the text. (For interpretation of the references to color in this figure, the reader is referred to the web version of this article.)

From the very beginning researchers observed features in the optical response of the QWs which suggested that indium is not randomly distributed (see for example [16,17]). Those findings were supported by theoretical calculations suggesting a low solubility of indium in GaN [7,18]. Different microscopy methods were employed [19–25] that probe for chemical inhomogeneities at near atomic resolution and build on a quantitative interpretation of image contrast or an extraction of composition-induced strain profiles.

Fig. 2 shows one of Nichia's commercially available products from the late 1990th. The packaged LED is smaller than a US dime and the square electronic chip positioned on top of a heat sink inside the packaged LED is about as wide as the thickness of the letters in the word "LIBERTY" of the dime. Such LED's are nowadays used in traffic lights, for example. Moreover, technology allows to disassemble such devices to recover information down to the atomic level as shown in the attached movie (Supplemental information). Reverse engineered and magnified further, one can see the metal contacts on top of the light emitting epilayers (blue square in Fig. 2). After preparation of a cross-sectional TEM sample, the $In_xGa_{1-x}N$ layer becomes visible as a dark line that is covered by an $Al_yGa_{1-y}N$ capping layer. The indium concentration that is relevant in this contribution is $x < 0.25$. It is pointed out that in early publications it was thought that x must be chosen twice as large for green light emission [26] before the existence of an inaccurate calibration was pointed out by electron microscopy [27]. The emission of blue or green light depends on the quantum well width as well as on growth parameters [6].

Supplementary material related to this article can be found online at: http://dx.doi.org/10.1016/j.mssp.2016.07.011.

This paper contains two main parts. Section 2 reviews the historical evolution of approaches that were pursued to detect indium clusters in $In_xGa_{1-x}N$ quantum wells including pattern recognition procedures, strain mapping, and the emerging opportunity to identify the substitution of gallium atoms with indium atoms by contrast measurements of single atomic columns. Section 3 proceeds describing ongoing improvements of electron microscopic investigations and their impact on understanding the nature of "indium clustering" at truly atomic resolution before the paper is concluded.

2. Quantification of indium clusters

2.1. Pattern recognition

In 1997 a Berkeley – Nichia collaboration produced a first map of the indium distribution in Nakamura's green light emitting QWs [26] utilizing QUANTITEM [20]. The mapping of the indium distribution from high resolution images was enabled by several achievements.

First, a quantitative analysis of image contrast in transmission electron microscopy is commonly challenging because the dynamic electron scattering changes the recorded intensity patterns in atomic-resolution images in a similar manner if sample thickness or the chemical compositions vary across the field of view. Thus, useful information about compositional changes can only be extracted if the sample thickness is determined. For example in Ref. [26], QUANTITEM is used to compare the contrast of a chemically homogeneous material of determined thickness – in this case GaN – with the contrast of the chemically heterogeneous $In_xGa_{1-x}N$ with nominally x=0.43. For this purpose a sample preparation technique was developed which produced thin, atomically flat and clean samples using a final KOH etch [26]. Extraordinary images could be obtained from such thoroughly prepared samples as shown by a direct comparison of images from $In_xGa_{1-x}N$/GaN QWs taken directly after a final ion milling step using 2 kV Ar ions with a TEM image of a similar area after applying the wet chemical etch. Fig. 4 of Ref. [28] shows the stunning superiority of the latter preparation process introduced in 1997 where any residual damage caused by the sample preparation process is entirely removed. The resulting homogeneous sample thickness even allows to record high resolution images from $In_xGa_{1-x}N$ and GaN QW's with a contrast that makes a distinction of $In_xGa_{1-x}N$ from GaN hardly possible, which is advantageous if strain mapping experiments are pursued [21]. Certainly, any trace of electron-beam induced sample damage is absent from such images and would be immediately recognized if it was present.

Secondly, the 1997 paper [26] used data acquisition times as short as possible, with a maximal electron beam exposure time < 2 min. This culture was fostered because data acquisition using a minimal exposure of the material to the electron beam was known to be a necessity, at least since 1990 [29]. Bulk group III – nitrides are radiation hard materials [30] if structural perfection is assumed. However, the presence of defects, surfaces and interfaces commonly soften the bulk binding energy of atoms and make the material more susceptible to damage. Unexpectedly, several microscopy groups re-visited this aspect but neglected to apply state-of-the-art sample preparation and minimized beam exposure [31–33]. Their conclusions, deduced from analyzing heavily damaged $In_xGa_{1-x}N$/GaN, created uncertainties which still shape research efforts nowadays [34].

In 2007 the Berkeley group started detailed studies of electron beam-sample interactions in $In_xGa_{1-x}N$ QWs. Bartel et al. compared the electron beam sensitivity of various semiconductor compounds and alloys. He found that in wet etched, clean TEM samples electron beam induced sample alterations are only negligible within the first minute of exposure time, for Si/SiGe, AlAs/GaAs, $In_xGa_{1-x}N$/GaN and AlGaN/GaN QWs. In such studies typical electron doses of a few thousand electrons per square Angstrom are delivered to record high resolution phase contrast images with an exposure time of around one second [35].

It is established knowledge that electrons accelerated by 100 kV to 300 kV, as commonly used for electron microscopy, preferentially damage the sample surfaces [36–38]. Atoms are displaced due to dominant knock-on events because atom binding energies at the surfaces are reduced compared to bulk values [39–41]. Rossell et al. [42] applied the model from McKinley and Feshbach [43] to calculate the total scattering cross section for a collision event between an electron and an atom embedded in a crystal. These cross sections σ_d are dependent on the acceleration energy of the electron, eU, the atomic number Z, the atom mass m_{atom} and the binding energy of the atom and read:

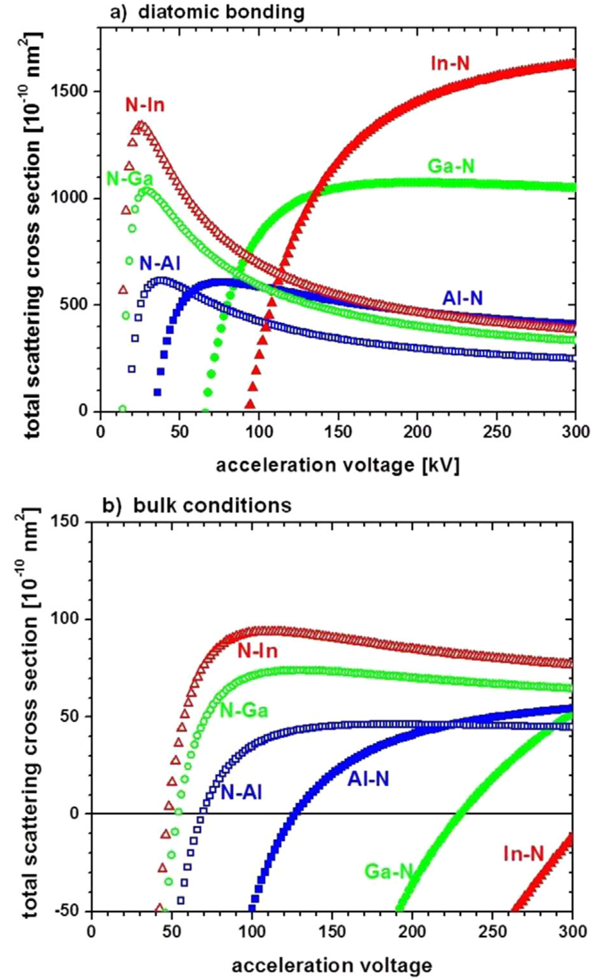

Fig. 3. Total scattering cross section σ_d for nitrogen atoms, bound to element X=(Al, Ga, In): "N-X" and element X=(Al, Ga, In), bound to nitrogen: "X-N"; for diatomic bonding (a) and bulk material (b). σ_d is shown dependent on the electron acceleration voltage.

$$\sigma_d = 10^{-14}\pi\frac{kg^2m^2}{C^4}\frac{e^4}{m_e^2}Z^2\frac{(1-\beta^2)}{\beta^4} \times\left[(\kappa-1)-\beta^2\ln\kappa+\pi\frac{Z}{137}\beta(2\sqrt{\kappa}-2-\ln\kappa)\right] \quad (1)$$

where e is the elementary charge, m_e the electron rest mass, β the relativistic speed of electron divided by speed of light, κ is an energy ratio $T_{max}/T_{d,\,min}$ with $T_{d,\,min}$ being the critical recoil energy for an atom displacement and T_{max} the maximal recoil energy that is given by:

$$T_{\max} = 4\frac{m_e}{m_{atom}}eU\left(1+\frac{eU}{2m_ec^2}\right) \quad (2)$$

Using Eqs. (1) and (2), the probability of displacing an atom in AlN, GaN and InN can be calculated if the binding energy is known. Taking energy values per bond from Ref. [44] to be Al–N=2.88 eV, Ga–N=2.2 eV and In–N=1.93 eV, two extreme cases are plotted in

Fig. 3. Fig. 3a shows how σ_d depends on the microscope's acceleration voltage for the surface condition where an atom is only bound to one other neighboring atom (diatomic bonding case) while Fig. 3b shows the total scattering cross section for the case of perfect bulk material where each atom is bound to four next neighbors in a tetrahedral configuration.

The graphics in Fig. 3 give valuable information about an optimized operation of electron microscopes. It is seen from Fig. 3b that bulk damage of InN is negligible even if an acceleration voltage of 300 kV is used. In fact, bulk displacement damage to all group III-nitrides can be entirely avoided if acceleration voltages are reduced to 60 kV or less. Aberration corrected instruments that operate in this voltage range are now available [45,46]. In contrast, reduced binding energies in surface proximity move threshold values to much lower energy as shown in Fig. 3a and one expects that sharp threshold values cannot exist because binding energies commonly vary greatly at defects, interfaces and surfaces. Remarkably, one finds a "sweet spot" around 80 kV in the case of diatomic bonding, for all three group III - nitrides. The nitrogen atoms (open symbols) interact with electrons strongest around 30 kV while the interaction of the metal ions (full symbols) increases towards higher energy so that the probability of a knock-on event to occur is lowest around 80 kV for all elements. As the actual displacement event is the product between the electron dose and the scattering cross section, minimizing the dose rate will proportionally reduce beam damage. Coincidently, the current technology also provides a largest image contrast at a voltage of 80 kV [47]. This peak contrast value occurs because the image contrast increases with decreasing acceleration voltages as a result of the voltage dependent electron scattering process. The larger scattering angles at low voltages, however, require a more precise correction of residual lens aberrations, which is more challenging at low voltages and often not available. Thus, in today's best aberration-corrected electron microscopes the investigations of III-nitrides are performed with voltages around 80 kV where cross sections for atom displacements at surfaces, interfaces and defects are smallest and a largest signal can be harvested that allows minimizing the electron dose that is needed to create a desired signal above noise. Certainly, the fabrication of samples with extraordinary flat surfaces remains a key issue. In the past, short exposure times were used to contain electron beam-induced sample alterations and high acceleration voltage was needed to achieve the desired resolution.

Unfortunately, exposure times in literature largely exceed the mentioned "<2 min maximal exposure" rule, with O'Neill [33] exposing the material for 20 min to show that electron beam induced damage can alter the III-nitrides beyond recognition. Clearly, the effects observed in Refs. [31–33] describe electron beam-induced sample alterations in a material that was already pre-damaged by sample preparation. Obviously, they cannot provide relevant information about the homogeneity of the indium distribution in the $In_xGa_{1-x}N$ alloy itself and they cannot be compared with data produced by the Berkeley group.

Third, already the first paper on mapping indium segregation effects in $In_xGa_{1-x}N$ provided error bars for data extraction. They allowed to state beyond doubt that consistently the 2nd interface of the $In_xGa_{1-x}N$ QW was less abrupt than the first one with respect to the growth direction. The effect was attributed before to indium segregation during the growth process [48,49] and was repetitively observed afterwards [50,51]. Within an $In_xGa_{1-x}N$ QW that emitted green light [35], a fluctuation of the indium concentration of about one-third of its average concentration value was measured, which is much less than the beam-induced fluctuations, that were reported later [32]. The detected fluctuations are certainly well above any random distribution of the indium on gallium lattice sites. However, QUANTITEM makes use of pattern recognition to detect relative contrast changes within the unit cells of $In_xGa_{1-x}N$ that are projected into the image plane without providing absolute numbers [20]. In such a situation the size of the clusters can be measured to be a few nanometer large, but atomistic details of the cluster geometry remain hidden. Thus, the procedure captures the presence of indium inhomogeneities in the $In_xGa_{1-x}N$ QWs at a resolution of 0.3–0.5 nm but does not provide their detailed geometry at atomic resolution or absolute indium concentration values.

It is not unexpected for semiconductor alloys containing indium to observe cluster formation because the indium atom radius of 163 pm largely exceeds that of Ga (134 pm) or aluminum (125 pm) and strain fields become essential if element substitutions take place. In fact, the formation of clusters containing 2, 3 or more atoms was observed before in the InAs/GaAs system using scanning tunneling microscopy (STM) [52]. It was argued that the lattice mismatch of 7% in case of InAs / GaAs is large enough to induce anisotropic strain components that determine this behavior. In the InN–GaN alloy system the lattice mismatch between the binary compounds reaches 12% and it would be surprising to find that clustering effects are absent.

Summarizing, publications in the late 1990th provided valuable information about the inhomogeneous indium distribution in indium rich $In_xGa_{1-x}N$ QWs ($x\sim0.25$) by observing relative concentration fluctuations in the range of 30% compared to their average value. This translates for an average indium concentration of $x=0.25$ to a detected fluctuation of $\Delta x\sim8\%$. This nomenclature is found throughout this text and respective figures. The investigations established key requirements for the imaging of indium clusters by electron microscopy, which included sample preparation, data acquisition and data evaluation to provide reproducible results. The choice of acceleration voltages to capture suitable images is of concern. In the early studies [26] 800 kV was utilized, which produces displacement damage of heavy and light elements, but on a low level since displacement cross sections typically decrease if the voltage increases (see Fig. 3). It was confirmed [53] that within the 2 min time limit used to take images in the high voltage microscope, the cluster geometry remained unaffected.

Acceleration voltages were reduced when the one Ångstrom resolution barrier was broken [54–56] and atomic resolution imaging with mid-voltage electrons (100–300 kV) became main stream. New developments included advanced data evaluation, with exit wave reconstructions recovering phase images [57–59] that allow evaluating contrast changes quantitatively, on single atomic columns, in transmission electron microscopy (TEM). The advent of scanning transmission electron microscopy (STEM) provided a stronger Z-dependence of the contrast, with the contrast $C\sim Z^{1.7}$ instead of $C\sim Z^{0.67}$ for phase contrast microscopy. Nowadays, aberration correction is a key part of instrument developments because it boosted resolution and sensitivity. On the downside, the development added technical complexity to advanced electron microscopes [60]. Also, the shift to lower acceleration voltages made electron beam-induced object alterations a larger concern. Although the microscopes can be operated below threshold values for atom displacements from bulk lattice sites, material alterations still occur rapidly at sites of lowered binding energy such as defects, interfaces or surfaces.

2.2. Strain mapping

QUANTITEM evaluates contrast templates from one projected unit cell of an image to the next one so that a relative indium concentration fluctuation in $In_xGa_{1-x}N$ QWs is assessed and mapped. A natural improvement of such measurements calls for a determination of absolute concentration values while maintaining

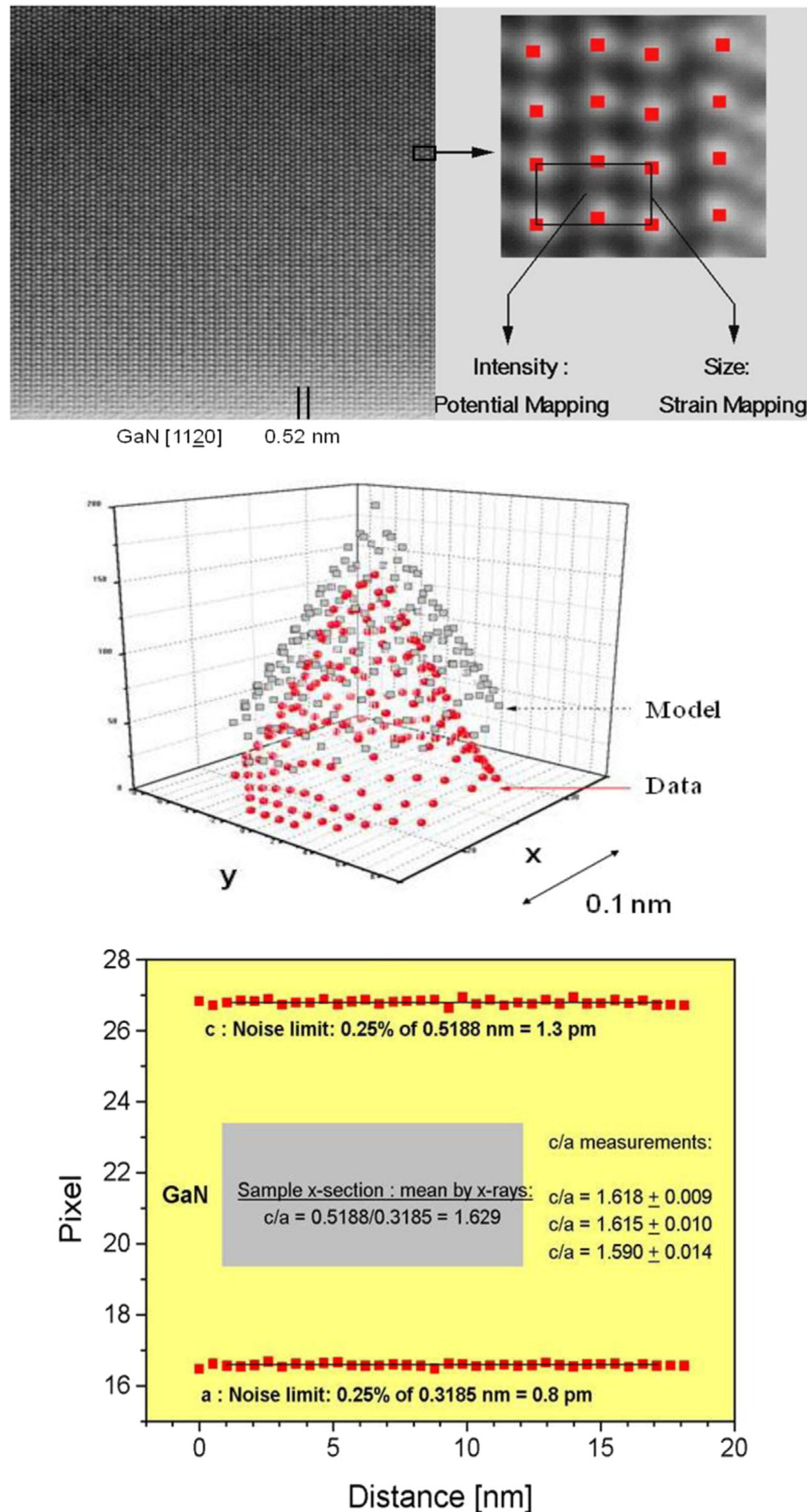

Fig. 4. Potential and strain mapping from high resolution images – Top: Experimental lattice image of a chemically etched GaN sample, 800 kV. The crystal unit cell is magnified. QUANTITEM evaluates the intensity distribution in the cell; strain mapping evaluates its size as indicated. – Middle: Intensity distribution of the model which determines the peak position of an atom column and data around each column position ("blob") – Bottom: Repetitive unit cell size measurements revealing a precision of ~1 pm. X-ray data were used to calibrate the sample.

the resolution that is set by the projected unit cells as shown in Fig. 4, top. A precise, local measurement of the projected lattice parameters in high resolution TEM images can provide this information and lead to the development of local strain measurements in high resolution TEM images, or Digital Atomic Resolution Image Processing (DARIP). This technique pinpoints the absolute positions of atom columns in suitably chosen HRTEM images, so that even tiny, local lattice constant changes can be detected. For this technique, the contrast around every atom column position is evaluated and a 2D contrast model is calculated which pinpoints

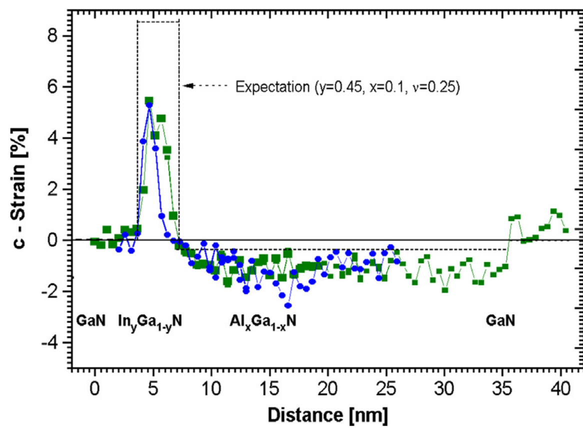

Fig. 5. Strain profile across a GaN/ $In_xGa_{1-x}N$/AlGaN/GaN quantum well structure showing the difference in c lattice parameter from the GaN epilayer, given in % strain. Also indicated as a box is the expected c-lattice strain from the nominal indium concentration of the green LED, as published in [26].

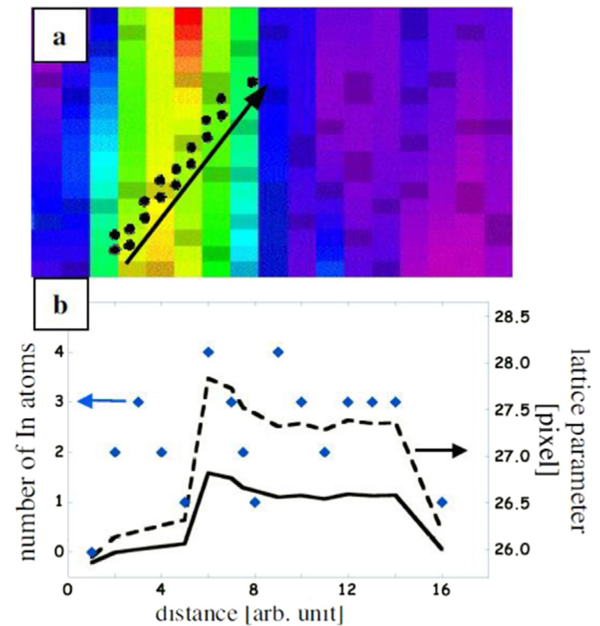

Fig. 6. A color-coded strain map across a GaN/$In_xGa_{1-x}N$/GaN QW (a) and the respective average strain profile across the quantum well (black lines in b)) The difference in the profile is due to potential strain relaxation effects in the thin sample. The relative changes in the lattice parameter are compared to the results of phase contrast interpretation as In replacing Ga atoms in the respective columns drawn as black dots in Fig. 6a. The spread of data points is high, for details see text.

the position of the atom column, as shown graphically in Fig. 4, middle. Local chemical compositions can be measured by the method if an element substitution causes strain as it is the case for the $In_xGa_{1-x}N$ system [27,61]. Fig. 4, bottom shows the precision as to which such measurements can be performed [21,61]. It is seen that repetitive measurements allow for a determination of column displacements in the range of 0.8 pm through 1.3 pm. In the $In_xGa_{1-x}N$ system this precision allows detecting indium fluctuations that exceed 0.02% [27,53]. Two aspects of such measurements are pointed out: The wavelength of electrons accelerated by 300 kV is 1.9 pm and becomes a limiting factor. An indium fluctuation of 0.02% corresponds to the substitution of one gallium atom by one indium atom in an atom column that is 50 atoms long. Since the atom spacing in [11–20] direction of the GaN is 0.32 nm, samples must at least be 16 nm thick to observe fluctuations on this level.

A detailed description of the requirements to reliably extract strain profiles from high resolution images is given in Ref. [62]. There, it is shown that the proportionality between indium concentration and resulting lattice constant c(x) can be approximated by $c(x)=0.5185+0.111x$ nm and that simulation of strain relaxation effects [61] must be employed to accurately describe the measured strain profiles across QW's for sample thicknesses up to 15 nm. Sample thickness is a critical parameter in these experiments. If it is chosen small, strain relaxation becomes very relevant; if chosen much thicker than the cluster diameter of a few nm, the material appears to be homogeneous. Further, the results revealed that even the best electron microscopes at this time could not unambiguously determine if clusters are formed in $In_xGa_{1-x}N$ alloys with $x\lesssim0.2$ because of their limited performance.

Concerning the $In_xGa_{1-x}N$ device structure of Fig. 2 the Fig. 5 shows the c lattice parameter variation across the active device area, which was extracted using the DARIP procedure [27,61] and can directly be converted into an indium concentration. It is assumed that the prepared TEM sample remained fully strained due to sufficient sample thickness [62]. Aluminum doping causes a lattice contraction while a substitution with indium atoms expands the GaN lattice as expected from the atomic radii of the elements. To the researchers' surprise, the maximum indium concentration in the two different LEDs was similar even though one device emitted green light while the other one emitted blue light. Obviously, this output energy difference is affected by quantum confinement since the blue LED had a quantum well width about half the size of the green LED as seen in Fig. 5. In addition, both materials contained $In_xGa_{1-x}N$ layers with about 22% of indium concentration, not nearly as high as the expected 43% [26]. Such results have immediate consequence on the fundamental band gap of $In_xGa_{1-x}N$, which was corrected to ~2.5 eV for $x=0.22$ in 2002 [63–65]. It was not taken into account, however, that the optical response in $In_xGa_{1-x}N$ alloys may be affected by quantum confinement, piezo-electric effects and/or cluster formation; the local concentration of indium due to fluctuations may be as high as 30% or $\Delta x=0.08$.

2.3. *Contrast quantification of single atom columns*

The investigation of $In_xGa_{1-x}N$ homogeneity is resolution dependent since the Ga-N separation is only 113 pm in a [11–20] projection image and only a few tenth of picometer larger if indium substitutes for gallium. This projected column separation could only be resolved with the introduction of the One Angstrom Microscope (OAM) in 2001, which was achieved by reconstructing electron exit wave functions from image series [66]. This holographic imaging tool recovers the electron exit wave functions using a Gerchberg-Saxton algorithm [67] and is described in references [57–59]. In addition, signal to noise ratios are boosted because the wave functions are reconstructed from image series that can contain hundreds of single micrographs. The algorithm is implemented in the commercially available McTempas software [68]. Certainly, this achievement opens the exciting perspective to increase the resolution to the ultimate limit of single atom columns.

Jinschek et al. presented such data in 2004 [24]. The samples were prepared using a focused ion beam (FIB), which had matured to be a valuable tool for site specific preparation of electron transparent specimens. The residual surface damage from the 30 kV (or 10 kV) Ga ion beam that is used for sample cutting was reduced with the already described wet chemical etch [26] to an approximately 1 nm thin amorphous layer. Focal series were taken

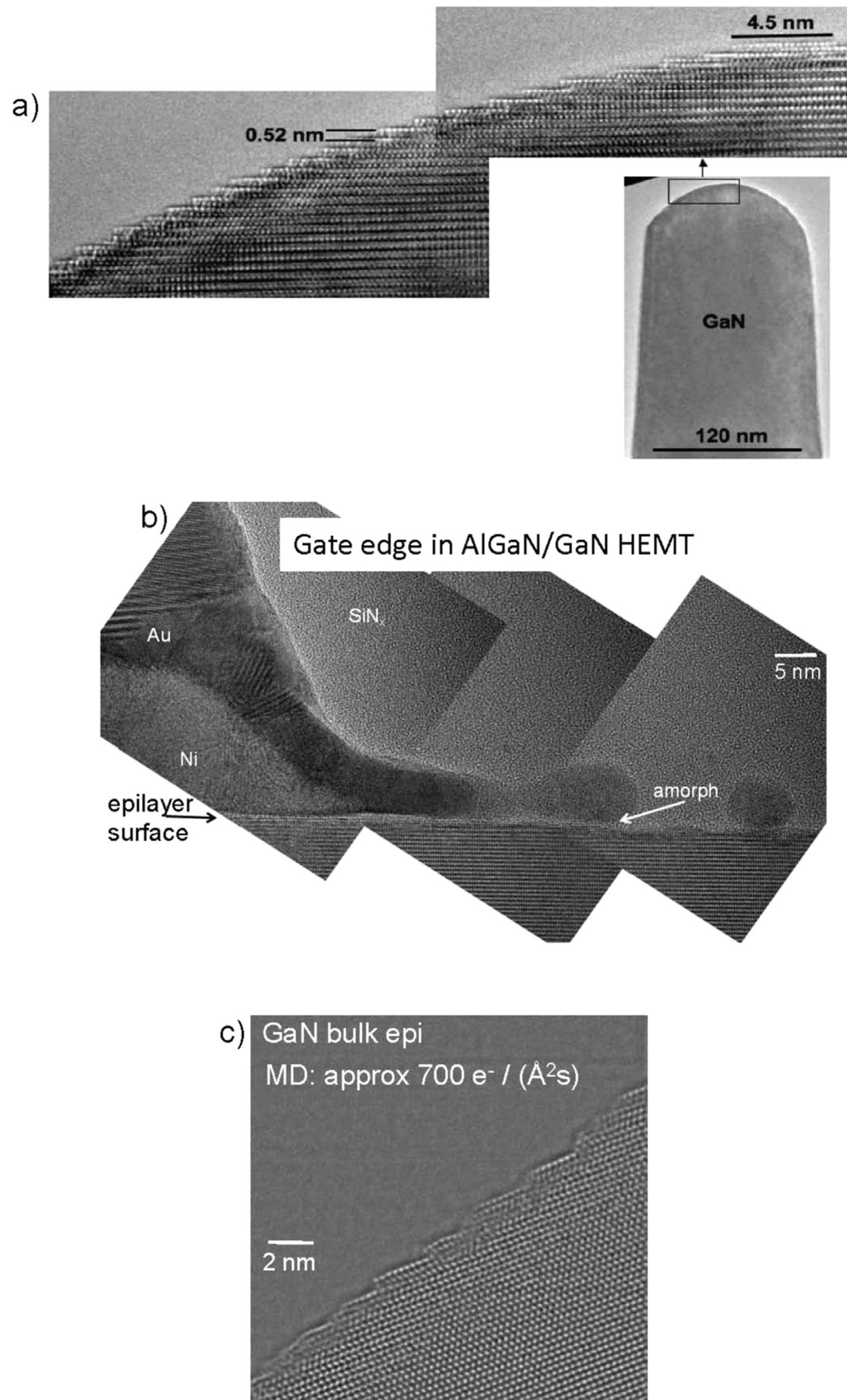

Fig. 7. "All ion-mill" sample preparation, using a standard Ga FIB process, with 900 eV Ar milling for further thinning and 500 eV Ar milling for a final cleaning step. a) GaN tip with atomically clean surface steps b) AlGaN/GaN HEMT structure, produced from complete, unpackaged device c) GaN bulk epi, for details see text.

from GaN/ $In_xGa_{1-x}N$/GaN quantum wells with approximately 17% of indium content and exit wave functions were reconstructed. In the related phase images any change in chemistry can be determined for atom column by atom column if the element specific phase change per atom can be measured (see Fig. 8 of Ref. [24]). A phase change per gallium atom of 0.145 rad was determined. For 1–4 indium atom substitutions in a thin sample area an expected phase difference between gallium and indium atoms of $\sim$0.125 rad was detected that barely exceeds noise levels. The resulting map of In atoms per atom column is plotted in Fig. 6 together with a strain profile taken from the same area. The exact locations of the atom columns which were used are shown as black dots in the strain map (Fig. 6a). An average indium concentration of 22% calculated from the strain map compares well with the average concentration obtained by the new phase contrast technique (23%). Both values exceeded the nominal indium concentration of 17%. The paper shows that phase changes can in principle be used to distinguish between In and Ga atoms in single atomic columns. The signal to noise ratio for the detection of single atoms, however, is poor and could only be enhanced by further improving on electron microscopy [69].

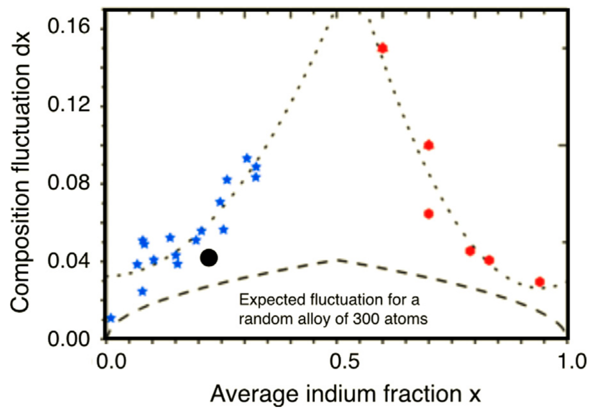

Fig. 8. Dependence of the indium composition fluctuation in GaN on the average indium fraction. Data are taken from Ref. [35]. The black circle marks the value of Baloch et al. Contributions from random alloy fluctuations were estimated in Ref. [35], too, and are too small to explain the measured fluctuations.

3. Improving the existing electron microscopy capabilities

3.1. FIB sample preparation

Nowadays, an "all ion-mill" sample preparation procedure is developed [70–72] that allows to fabricate atomically flat and clean surfaces without applying a chemical etch. In this process a standard FIB lift-out process is applied, first using a 30 kV Ga ion beam with gradually reducing beam currents from 3000 pA to 100 pA. No effort is made to thin the samples beyond a thickness of 250 nm to 300 nm. Instead, the final specimen thinning to electron transparency occurs in a low energy Ar ion mill (Nanomill, Fischione Inc.), which employs a 900 eV Ar beam first while the final cleaning step is performed at 500 eV. Before imaging the sample, a 1 min long plasma cleaning process removes any residual hydro-carbon contaminations that may originate from air exposure or from the sample holder itself. A standard 25% oxygen, 75% argon gas mixture is used. If the material is sensitive to oxygen exposure, only the empty holder is plasma cleaned, and the mounted sample undergoes a short Nanomill clean prior to imaging. Fig. 7 shows various examples of state-of-the-art prepared samples using this technique. Fig. 7a depicts a round needle where mono-atomic steps produce its shape. Any residual amorphous layer is absent. Fig. 7b demonstrates how the process can be used to investigate full device structures. Here, a Ni/Au gate edge on top of a AlGaN/GaN epilayer is shown. The existing amorphous layer is a SiN_x passivation layer, which is a part of the device structure and not a damage artifact from ion milling. The chemical stability along various interfaces was investigated which is a direct measure of thermal stability and radiation hardness of the device [71,72]. Any sample preparation artifacts can thereby mask diffusion processes. Lastly, in Fig. 7c a bulk GaN layer is imaged which contains residual surface implantation damage from a dopant implantation which is investigated. Again, there is no amorphous layer present. This preparation technique is a prerequisite for investigating indium fluctuations on a single atom level because poorly defined surfaces would falsify suitable high-resolution TEM or STEM investigations that aim at single atom sensitivity.

3.2. Valence electron energy loss spectroscopy (VEELS)

It is instructive to address the chemical homogeneity of the binary InN alloy first, which was investigated by Bartel et al. In this study, the InN was grown in an MBE system with an intentional temperature gradient across the wafer [73]. Samples from two extreme temperature regions were compared. Their respective photo-luminescence showed two distinctly different emission peaks at 0.55 and 0.7 eV. The latter emission is observed from a sample where indium precipitates with an average diameter of about 20 nm were found that contribute to a pronounced indium plasmon peak at 11.2 eV energy in VEELS spectra. However, the other sample did not contain these large metal precipitates. Instead, much smaller indium atom clusters were present with only ~5 nm cluster diameter that escape observations by many other advanced material characterization techniques. Only advanced microscopy techniques, with aberration-corrected lenses, dose-controlled imaging and perfect sample preparation may be able to reveal the detailed atomic structure of even smaller inclusions, with diameters ~2 nm. There is no doubt, however, that their presence affects the optical properties of InN because the optical emission energies are shifted from 0.7 eV to 0. 55 eV.

VEELS spectra of $In_xGa_{1-x}N$ alloys and InN consistently showed higher band gap energies than observed by optical absorption and PL [63–65] if they are extracted from "quasi-bulk" areas. In contrast, the band gap energies seem reduced in the proximity of surfaces or InN/GaN, and InN/Al_2O_3 interfaces to values around 1.0 and 0.8 eV, respectively. Wurtzite InN exhibits a band gap energy around 1.7 eV [74,75] while zincblende InN features a 1.4 eV bandgap. These energies were measured to an accuracy of ~0.2 eV. When conducting VEELS experiments it is likely that the high beam current causes local heating, which would reduce the measured bandgap energy [76]. Therefore, the extracted energy data may describe a lower limit.

Nevertheless, close to interfaces or surfaces the energy values are consistently measured close or below 1.0 eV. This finding also matches optical measurements of InN nanowires and quantum dots. Those structures which consist of large surface areas also show reduced optical bandgap values, in the vicinity of 1.0 eV [77–80]. The mostly cited bandgap of 0.7 eV for InN [63] may therefore very well be its optical bandgap, but it is not at all clear if this is also its fundamental bandgap [81].

Local indium fluctuations in combination with band gap (Eg) variations were observed in high efficiency green light emitting $In_xGa_{1-x}N$/GaN diodes by Jinschek et al. [82]. The authors analyzed VEELS data to find emission energies that peak at Eg=3.13 eV, with a variance towards lower energies of ΔEg=0.20 eV (asymmetric distribution). These data suggest an average indium content of x=0.15%, along the majority area of the quantum well, with a fluctuation of Δx=0.07%. The indium is enriched in clusters of 1–3 nm size, with indium concentrations of x=0.30 to x=0.4. Corresponding to those small clusters, energy tails of Eg=2.65 eV were observed in the VEEL spectra. This energy feature is consistent with the observed light emission in the LED, but is only observed in a small fraction of the quantum well. It was demonstrated for the first time that this inhomogeneity can be quantified by local strain measurements and by local variations of the $In_xGa_{1-x}N$ band gap energy in a quantum well that is 3.0 ± 0.5 nm of average width, with the lower interface to be more abrupt than the upper one. The data is consistent with the view that the fundamental band gap of InN is high [74,75]. These results would also explain the low efficiency of green LEDs, as the "active" areas of enriched $In_xGa_{1-x}N$ are small compared to the quantum well area.

3.3. Prospects for aberration-corrected microscopy

In 2009 DOE's TEAM project was successfully concluded [83] and contributed to foster aberration-corrected electron microscopy in the US and around the world. Investigations of $In_xGa_{1-x}N$ alloys, however, did not benefit from this development until 2013 when K.H. Baloch et al. revisited the indium clustering question in $In_xGa_{1-x}N$ using aberration-corrected electron microscopy at

120 kV [34]. The authors confirmed that the"gross indium clustering" is indeed nothing but a consequence of beam-sample interactions. They used VEELS measurements to conclude that "indium clustering is not present in as-grown $In_{0.22}$ $Ga_{0.78}N$ QWs", which is unexpected because it contradicts the data shown in Fig. 8.

However, an assessment can be made concerning the validity of the statement by directly comparing the mean indium concentration value and its fluctuation with the literature data of Fig. 8. It summarizes electron microscopy data of samples from a variety of sources including Lumileds, Aixtron, Nichia and others, that were grown during the years 1997–2005 [27,35]. From the letter of Baloch et al. [34], the listed indium concentration of 22% and assigned errors ranging from 3% to 5.4% are used to add a single data point at $x/y=0.22/\sim 0.04$ to the Fig. 8 (full black circle). A striking agreement of this data point with previously published strain results is immediately revealed that is also consistent with the previous indium fluctuation measurements by VEELS [82]. These outstanding agreements of independent data sets strongly supports the cluster model but are in stark contradiction to the opposite statement that was made in the letter. Such misunderstandings originate from the assignment of the relatively small composition variations to be "due to the statistical fluctuations of a random alloy", which is not a valid assumption as shown in Fig. 8 but often adopted without providing proof for the claim. A direct, quantitative comparison of the random alloy fluctuation of aluminum in GaAs with the indium cluster formation in GaN was made in Ref. [53]. This comparison is revealing because the negligible lattice mismatch between AlAs and GaAs does not induce local strain components as it is the case for the InAs/GaAs and even more for the InN/GaN alloy systems.

It is satisfying that a coherent picture emerges by now with the following core aspects:

a) In the past, electron beam-induced sample alterations could already be minimized by best practices so well that the image quality already matched the needs of today's aberration-corrected electron microscopy. Exceptions from this practice are known, e.g. [31,32], although they were surprisingly long debated.

b) An intrinsic "data scatter" is present in all investigations that aim at measuring indium fluctuation. It's consistency reveals that the available experimental approaches operate at the threshold to detect indium fluctuations but are mostly not sensitive enough to make reliable statements about the statistical distribution of indium atoms in GaN. To date, strain measurements have provided the most consistent results that show the formation of indium clusters on a length scale of a few nm [53]. Such measurements, nevertheless, depend on the sample thickness, for thick layers (e.g. in Ref. [84]) fluctuations will be averaged.

c) The indium distribution in $In_xGa_{1-x}N$ layers that are used in LED's does not grossly differ from material to material if fabricated by different sources. Therefore, the behavior of indium in GaN likely reflects an intrinsic materials property such as spinodal decomposition [35].

d) Indium atoms in GaN are not randomly (Poisson) distributed but seem to cluster in preferential arrangements in the c plane of the wurtzite structure. An experimental indium distribution at atomic resolution was published in Ref. [28]. Similar atom arrangements were detected at $In_xGa_{1-x}N$/GaN interfaces and were called "quantum disks" [85].

Obviously, the known benefit of carrier localization in indium rich regions recently gained renewed attention [86]. However, further progress to determine the atomistic distribution of indium atoms in the GaN matrix became only recently possible. It requires the application of emerging new tools that greatly expand the current abilities of aberration-corrected electron microscopy by increasing the sensitivity for the detection of single atoms by a factor of 2–3 and by minimizing beam-sample interactions through dose-rate and illumination control [87]. It can even be expected that single indium atoms can be located in 3D [88].

3.4. What is the atomic structure of "indium clusters"?

The low band gap of InN, in combination with high optical absorption, makes the material attractive for photovoltaic applications. Certainly, the prospect of covering the whole visible light spectrum using only the $In_xGa_{1-x}N$ ternary semiconductor alloy, is exciting. However, InN is a quite unusual semiconductor: For the group III–V semiconductors (Al, Ga, In)–(N,P, As, Sb) the band gap is generally reduced when an element is replaced with one of higher atom number Z. InN is the only exception, with $E_{bandgap}$ (InP) > $E_{bandgap}$ (InN). This exception was suggested in 2001 when Wu et al. published a corrected value of 0.7 eV for the InN fundamental band gap [89]. Originally, the InN band gap was given to be 1.9 eV (see for example [90]). When optical responses in the $In_xGa_{1-x}N$ system showed a reduced emission energy for averaged indium concentrations, the energy value for the binary compound was reduced as well [63–65,89,91]. Also, InN exhibits the highest equilibrium nitrogen partial pressure among the group III – nitrides [3]. The latter results in a general inability to grow InN crystals at high temperatures, unless one uses multiple atmospheric nitrogen pressure conditions [92,93]; the crystals are commonly grown at temperatures around 500 C. The material's absorption is very high, likely due to the presence of defects in the material in magnitudes as large as $10^{20}/cm^3$[94]. A large concentration of nitrogen vacancies, V_N, was predicted by theory [95], up to several $10^{18}/cm^3$ V_{In} were measured in positron annihilation spectroscopy, accumulated at interfaces [96]. However, little is known how this large concentration of native defects evolves across the $In_xGa_{1-x}N$ ternary alloy system and how it is modified during observations in an electron microscope.

In 2003 part of the scientific community focused on the debate about indium clusters in $In_xGa_{1-x}N$ on what can be described as "gross indium fluctuations" [31–33]. Large structural features were detected by strain measurements that would require the presence of indium fluctuation values $\Delta x > 50\%$. They were created by intentional (and unintentional) electron irradiation of samples that contained only moderate indium concentration around $x \sim 0.2$. Strain measurements were used to detect these features that resembled the previously reported, but much lower indium fluctuations in the range of $0.03 < \Delta x < 0.09$. These investigations casted doubt on the validity of the earlier measurements even though they disregarded the established, best practices to capture electron micrographs without introducing damage as well as the need for superior sample preparation. It is of cause entirely uncertain what the nature of the defects is that create the "gross" fluctuations that were picked up by strain measurements and attributed to the formation of indium clusters simply because of a similar feature size.

In particular, the time evolution of indium clusters became an issue, which relates to the total electron dose that is needed to inflict beam-induced sample alterations. In light of this debate, Bartel et al. revisited the question if pristine indium-rich clusters change when imaged at 150 kV and 300 kV instead of using 800 kV as pursued previously. It was found that similar time constraints apply that allow reproducing the earlier results if the above described measurement conditions are respected [53]. In particular, it was re-established that the indium fluctuations increase with increasing indium content in $In_xGa_{1-x}N$ for $x < 0.3$ as published in Ref. [27] and shown in figure 8 [35]. Further, indium fluctuation measurements were extended to include larger indium concentrations $x > 0.5$. The investigation showed that phase separation by spinodal decomposition provides a consistent way to describe cluster formation across the whole compositional range

$0 < x < 1$ and that one must expect a quasi-periodic cluster formation in $In_xGa_{1-x}N$ QWs because spinodal decomposition is confined by the well geometry as pointed out by Kenzler et al. [97].

It is of interest to discuss the nature of the observed fluctuations. If one considers that a fluctuation necessarily creates a deviation from a random distribution of indium atoms on gallium lattice sites, it seems desirable to directly measure this deviation. However, it was pointed out before that it was technologically barely feasible to reliably isolate the contrast of single indium atoms in the GaN matrix and a location of single indium atoms in three-dimensions was certainly beyond reach. Nevertheless, several investigations frame the range of parameters that must be met. To our knowledge, only reference [35] showed that the assumption of a random indium distribution directly conflicts with the fluctuation measurements across the entire composition range $0 < x < 1$ as shown in Fig. 8. Certainly, all measurements of "gross indium fluctuations" [31–33] do not relate to pristine material properties but to electron beam-induced sample alterations and one may speculate what type of defects are formed during this process that create these structures. On the other hand, a credible picture emerged that pristine indium-rich clusters tend to be constructed from plate-like structures in the [0001] basal planes of the GaN crystal [98] that is nowadays pursued. The fact remains that technological limitations of electron microscopy did not allow to develop a detailed description of the clustering process as it was achieved for the case of the InAs/GaAs QW's using scanning tunneling microscopy [52], where it was shown that the clustering is driven by strain fields. Such strain fields, however, are different in the cubic (InAs/GaAs) and the hexagonal (InN/GaN) alloy systems.

4. Conclusions

Optical and electrical properties of $In_xGa_{1-x}N$ alloys as well as its binary compound InN are influenced by the materials' homogeneity or the lack thereof. A tendency for phase segregation in this system is undisputed. Therefore, the formation of "indium clusters" in $In_xGa_{1-x}N$ alloys is to be expected and their presence is indeed consistently observed, in particular, if lattice matched and strained QW structures are investigated. However, the term "indium cluster" is used to describe an undetermined variety of precipitates of unknown structure and chemical composition. It reflects the inability to perform structural investigations with single atom sensitivity in three dimensions without actively altering their pristine structure during the observations in electron microscopes. Evidence has emerged that they are formed from plate-like precipitates in the basal plane of the wurtzite structure. Today's most advanced electron microscopy techniques must be employed and only those can improve this situation by finally solving the mysteries still surrounding this alloy system.

Acknowledgments

The authors acknowledge support through the US Department of Energy, National Nuclear Security Administration, Office of Defense Nuclear Nonprofileration R&D, under research Grant #FP00002844. The sample preparation of the GaN needle, shown in Fig. 7a, was performed by D. Detert, MSE, UCB; the "all ion mill" sample preparation was developed under a project from the Defense Threat Reduction Agency, #DTRA-253-HDTRA-122227. The use of electron microscopy facilities in the Molecular Foundry of LBNL, was supported by the Office of Science, Office of Basic Energy Sciences, of the U.S. Department of Energy under Contract No. DE-AC02-05CH11231.

References

[1] ⟨http://www.ledinside.com/news/10/2014/⟩ the_story_behind_-shuji_nakamuras_invention_of_blue_leds and S. Nakamura, T. Mukai, M. Senoh, Appl. Phys. Lett., vol. 69(1680), 1996, 10.1063/1.117026.
[2] H. Amano, M. Kito, K. Hiramatsu, I. Akasaki, Jpn. J. Appl. Phys. 28 (1989) L2112.
[3] O. Ambacher, J. Phys. D Appl. Phys. 31 (1998) 2653.
[4] C. Kisielowski, J. Kruger, S. Ruvimov, et al., Phys. Rev. B 54 (1996) 17745.
[5] H. Amano, S. Kamiyama, I. Akasaki, Proc. IEEE 90 (2002) 1015.
[6] N.A. Shapiro, P. Perlin, C. Kisielowski, L.S. Mattos, J.W. Yang, E.R. Weber, MRS Internet J. Nitride Semicond. Res. 5 (2000) 1.
[7] I.H. Ho, G.B. Stringfellow, Mater. Res. Soc. Proc. 449 (1997) 871.
[8] D. Doppalapudi, S.N. Basu, K.F. Ludwig, T.D. Moustakas, J. Appl. Phys. 84 (1998) 1389.
[9] N.A. El-Masry, E.L. Piner, S.X. Liu, S.M. Bedair, Appl. Phys. Lett. 72 (1998) 40.
[10] K.P. O'Donnell, R.W. Martin, P.G. Middleton, Phys. Rev. Lett. 82 (1999) 237.
[11] C.A.M. Fabien, B.P. Gunning, W.A. Doolittle, A.M. Fischer, Y.O. Wei, H. Xie, J. Cryst. Growth 425 (2015) 115.
[12] M. Moseley, B. Gunning, J. Greenlee, J. Lowder, G. Namkoong, W.A. Doolittle, J. Appl. Phys. 112 (2012) 014909.
[13] S. Nakamura, M. Senoh, N. Iwasa, S. Nagahama, Jpn. J. Appl. Phys. 34 (1995) L797.
[14] ⟨https://webofknowledge.com/⟩.
[15] H. Zhao, G. Liu, J. Zhang, J.D. Poplawsky, V. Dierolf, N. Tansu, Opt. Express 19 (2011) A991.
[16] S. Chichibu, T. Asuhata, T. Sota, S. Nakamura, Appl. Phys. Lett. 69 (1996) 4188.
[17] Y. Narukawa, Y. Kawakami, Sz Fujita, Sg Fujita, S. Nakamura, Phys. Rev. B 55 (1997) 1938R.
[18] S. Keller, B.P. Keller, D. Kapolnek, et al., Appl. Phys. Lett. 68 (1996) 3147.
[19] S. Kret, P. Ruterana, A. Rosenauer, Phys. Stat. Sol. 227 (2001) 247.
[20] C. Kisielowski, P. Schwander, F.H. Baumann, M. Seibt, Y. Kim, A. Ourmazd, Ultramicroscopy 58 (1995) 131.
[21] C. Kisielowski, O. Schmidt, Microsc. Microanal. 4 (1998) 614.
[22] M.J. Hytch, E. Snoeck, R. Kilaas, Ultramicroscopy 74 (1998) 131.
[23] H. Lakner, Q. Liu, G. Brockt, et al., Mater. Sci. Eng. B 51 (1998) 44.
[24] J.R. Jinschek, C. Kisielowski, D. Van Dyck, P. Geuens, Proc. SPIE Int. Soc. Opt. Eng. 5187 (2004) 54.
[25] J.S. Barnard, M.E. Vickers, M.J. Kappers et al., Inst. Phys. Conf. Ser., vol. 180, 2004, p. 57.
[26] C. Kisielowski, Z. Liliental-Weber, S. Nakamura, Jpn. J. Appl. Phys. 36 (1997) 6932.
[27] C. Kisielowski, Proc. 2nd Internat. Symp. on Blue Laser and Light Emitting Diodes, Chiba, Japan, Ohmsha Ltd., 1998, p. 321.
[28] C. Kisielowski, T.P. Bartel, P. Specht, F.-R. Chen, T.V. Shubina, Physica B 401–402 (2007) 639.
[29] B. Deveaud, B. Guenais, A. Poudoulec, A. Regreny, C. d'Anterroches, Phys. Rev. Lett. 65 (1990) 2317.
[30] A. Ionascut-Nedelcescu, C. Carlone, A. Houdayer, H.J. von Bardeleben, J. C. Cantein, S. Raymond, IEEE Trans. Nucl. Sci. 49 (2003) 2733.
[31] T. Li, E. Hahn, D. Gerthsen, A. Rosenauer, A. Strittmatter, L. Reissmann, D. Bimberg, Appl. Phys. Lett. 86 (2005) 241911.
[32] T.M. Smeeton, M.J. Kappers, J.S. Barnard, M.E. Vickers, C.J. Humphreys, Appl. Phys. Lett. 83 (2003) 5419.
[33] J.P. O'Neill, I.M. Ross, A.G. Cullis, T. Wang, T.J. Parbrook, Appl. Phys. Lett. 83 (2003) 1965.
[34] K.H. Baloch, A.C. Johnston-Peck, K. Kisslinger, E.A. Stach, S. Gradečak, Appl. Phys. Lett. 102 (2013) 191910.
[35] T.P. Bartel, P. Specht, J.C. Ho, C. Kisielowski, Philos. Mag. 87 (2007) 1983.
[36] D.J. Smith, M.R. McCartney, Ultramicroscopy 23 (1987) 299.
[37] P.E. Batson, N. Dellby, O.L. Krivanek, Nature 418 (2002) 617.
[38] A.V. Martin, K. Ishizuka, C. Kisielowski, L.J. Allen, Phys. Rev. B 74 (2006) 172102.
[39] N. Jiang, J.C.H. Spence, Ultramicroscopy 113 (2012) 77.
[40] R. Egerton, P. Li, M. Malac, Micron 35 (2004) 399.
[41] C. Kisielowski, Adv. Mater. 27 (2015) 5838.
[42] M.D. Rossell, R. Erni, M. Asta, V. Radmilovic, U. Dahmen, Phys. Rev. B 80 (2009) 024110.
[43] W.A. McKinley, H. Feshbach, Phys. Rev. 74 (1948) 1759.
[44] H. Morkoc, Handbook of Nitride Semiconductors and Devices, 1, WILEY-VCH Verlag GmbH & Co KGaA, Weinheim, Germany, 2008.
[45] O.L. Krivanek, N. Dellby, M.F. Murfitt, M.F. Chisholm, T.J. Pennycook, K. Suenaga, V. Nicolosi, Ultramicroscopy 110 (2010) 935.
[46] B. Barton, B. Jiang, C. Song, P. Specht, H. Calderon, C. Kisielowski, Microsc. Microanal. 18 (2012) 982.
[47] C. Kisielowski, L.-W. Wang, P. Specht, J.H. Kang, R. Cieslinski, Microsc. Microanal. 19 (2013) 1210.
[48] S.S. Dosanjih, X.M. Zhang, D. Sansom, J.J. Harris, M.R. Fahy, B.A. Joyce, J.B. Clegg, J. Appl. Phys. 74 (1993) 2481.
[49] D.A. Gruetzmacher, T.O. Sedgwick, A. Powell, M. Tejwani, S.S. Iyer, J. Cotte, F. Cardone, Appl. Phys. Lett. 63 (1993) 2531.
[50] C. Kisielowski, Gallium nitride, in: J.I. Pankove (Ed.), Semiconductors and Semimetals, 57, T.D. Moustakas_Academic, London, 1999, p. 311, Fig. 30.
[51] C. Kisielowski, Gallium nitride, in: J.I. Pankove (Ed.), Semiconductors and Semimetals, 57, T.D. Moustakas_Academic, London, 1999, p. 307, Fig. 2.
[52] J.F. Zheng, J.D. Walker, M.B. Salmeron, E.R. Weber, Phys. Rev. Lett. 72 (1994)

2414.
[53] T. Bartel, J.R. Jinschek, B. Freitag, P. Specht, C. Kisielowski (Eds.), Phys. Stat. Sol (a), 203, 2006, p. 167.
[54] M. Haider, S. Uhlemann, E. Schwan, H. Rose, B. Kabius, K. Urban, Nature 392 (1998) 768.
[55] P.D. Nellist, S.J. Pennycook, Phys. Rev. Lett. 81 (1998) 4156.
[56] C. Kisielowski, E.C. Nelson, C. Song, R. Kilaas, R. Thust, Microsc. Microanal. 6 (2000) 16.
[57] W.M.J. Coene, A. Thust, M. Op de Beeck, D. Van Dyck, Ultramicroscopy 64 (1996) 109.
[58] A. Thust, W.M.J. Coene, M. Op de Beeck, D. Van Dyck, Ultramicroscopy 64 (1996) 211.
[59] W.K. Hsieh, F.-R. Chen, J.J. Kai, A.I. Kirkland, Ultramicroscopy 98 (2004) 99.
[60] C. Kisielowski, P. Specht, S.M. Gygax, B. Barton, H.A. Calderon, J.H. Kang, R. Cieslinski, Micron 68 (2015) 186.
[61] C. Kisielowski, O. Schmidt, J. Yang, Mat. Res. Soc. Symp. Proc., vol. 482, 1998, p. 369.
[62] T.P. Bartel, C. Kisielowski, Ultramicroscopy 108 (2008) 1420.
[63] J. Wu, W. Walukiewicz, K.M. Yu, J.W. Ager III, E.E. Haller, H. Lu, W.J. Schaff, Appl. Phys. Lett. 80 (2002) 4741.
[64] P. Ryan, C. McGuinness, J.E. Downes, K.E. Smith, D. Doppalapudi, T. D. Moustakas, Phys. Rev. B 65 (2002) 205201.
[65] V.Yu Davydov, A.A. Klochikhin, R.P. Seisyan, V.V. Emtsev, et al., Phys. Stat. Sol. B 229 (2002) R1.
[66] C. Kisielowski, C.J.D. Hetherington, Y.C. Wang, R. Kilaas, M.A. O'Keefe, A. Thust, Ultramicroscopy 89 (2001) 243.
[67] R.W. Gerchberg, W.O. Saxton, Optik 35 (1972) 237.
[68] 〈https://www.totalresolution.com/〉.
[69] C. Kisielowski, B. Freitag, M. Bischoff, et al., Microsc. Microanal. 14 (2008) 469.
[70] T.J. Anderson, A.D. Koehler, M.J. Tadjer, K.D. Hobart, P. Specht, M. Porter, T. R. Weatherford, B. Weaver, F.J. Kub, ECS Transactions 58 (2013) 221.
[71] A. Koehler, P. Specht, T.J. Anderson, B.D. Weaver, J.D. Greenlee, M.J. Tadjer, M. Porter, M. Wade, O.D. Dubon, K.D. Hobart, T.R. Weatherford, F.J. Kub, IEEE Electron. Dev. Lett. 35 (2014) 1194.
[72] J.D. Greenlee, P. Specht, T.J. Anderson, A.D. Koehler, B.D. Weaver, M. Luysberg, O.D. Dubon, F.J. Kub, T.R. Weatherford, K.D. Hobart, Appl. Phys. Lett. 107 (2015) 083504.
[73] T.P. Bartel, C. Kisielowski, P. Specht, T.V. Shubina, V.N. Jmerik, S.V. Ivanov, Appl. Phys. Lett. 91 (2007) 101908.
[74] P. Specht, J. Ho, X. Xu, R. Armitage, E.R. Weber, R. Erni, C. Kisielowski, Solid State Comm. 135 (2005) 340.
[75] P. Specht, J.C. Ho, X. Xu, R. Armitage, E.R. Weber, R. Erni, C. Kisielowski, J. Cryst. Growth 288 (2006) 225.
[76] N. Nepal, J. Li, M.L. Nakarmi, J.Y. Lin, H.X. Jiang, Appl. Phys. Lett. 87 (2005) 242104.
[77] T. Inushima, V.V. Mamutin, V.A. Vekshin, S.V. Ivanov, T. Sakon, M. Motokawa, S. Ohoya, J. Cryst. Growth 227–228 (2001) 481.
[78] B. Maleyre, O. Briot, S. Ruffenach, J. Cryst. Growth 269 (2004) 15.
[79] T.V. Shubina, S.V. Ivanov, V.N. Jmerik, et al., Phys. Rev. Lett. 92 (2004) 117407.
[80] T. Kuykendall, P. Ulrich, S. Aloni, P. Yang, Nat. Mater. 6 (2007) 951.
[81] P. Specht, W. Hong, E.R. Weber, MRS Symp. Proc. 994 (2007), F02-01.
[82] J.R. Jinschek, R. Erni, N.F. Gardner, A.Y. Kim, C. Kisielowski, Sol. State Comm. 137 (2006) 230.
[83] U. Dahmen, R. Erni, V. Radmilovic, C. Kisielowski, M.-D. Rossell, P. Denes, Philos. Trans. R. Soc. A - Mat. Phys. Eng. Sci. 367 (2009) 3795.
[84] A. Rosenauer, D. Gerthsen, V. Potin, Phys. Stat. Sol. (a) 203 (2006) 176.
[85] N.K. van der Laak, R.A. Oliver, M.J. Kappers, C.J. Humphreys, Appl. Phys. Lett. 90 (2007) 121911.
[86] R.A. Oliver, F.C.-P. Massabuau, M.J. Kappers, W.A. Phillips, E.J. Thrush, C. C. Tartan, W.E. Blenkhorn, T.J. Badcock, P. Dawson, M.A. Hopkins, D.W. E. Allsopp, C.J. Humphreys, Appl. Phys. Lett. 103 (2013) 141114.
[87] C. Kisielowski, L.-W. Wang, P. Specht, H.A. Calderon, B. Barton, B. Jiang, J. H. Kang, R. Cieslinski, Phys. Rev. B 88 (2013) 024305.
[88] F.-R. Chen, D. Van Dyck, C. Kisielowski, vol. 10603, 2016. 〈www.nature.com/DOI:10.1038/ncomms〉.
[89] J. Wu, W. Walukiewicz, K.M. Yu, J.W. Ager III, E.E. Haller, H. Lu, W.J. Schaff, Y. Saito, Y. Nanishi, J. Cryst. Growth 227–228 (2001) 481.
[90] T.L. Tansley, C.P. Foley, J. Appl. Phys. 59 (1986) 3241.
[91] Y. Saito, N. Teraguchi, A. Suzuki, T. Araki, Y. Nanishi, Jpn. J. Appl. Phys. 40 (2001) L90.
[92] I. Grzegory, J. Jun, S. Krukowski, P. Perlin, S. Porowski, Jpn. J. Appl. Phys. 32 (1993), suppl. 32-1.
[93] G. Darkaya, M. Buegler, R. Atalay, et al., Phys. Stat. Sol. (a) 207 (2010) 1379.
[94] G.M. Martin, Appl. Phys. Lett. 39 (1981) 747.
[95] C. Stampfl, C.G. Van de Walle, D. Vogel, P. Kruger, J. Pollmann, Phys. Rev. B 61 (2000) R7846.
[96] A. Laakso, J. Oila, A. Kemppinen, K. Saarinen, W. Egger, L. Liszkay, P. Sperr, H. Lu, W.J. Schaff, J. Cryst. Growth 269 (2004) 41.
[97] R. Kenzler, F. Eurich, P. Maass, et al., Comput. Phys. Comm. 133 (2001) 139.
[98] J.R. Jinschek, C. Kisielowski, Physica B 376 (2006) 536.